

## “Eastonite” from Easton, Pennsylvania: A mixture of phlogopite and a new form of serpentine

KENNETH J. T. LIVI, DAVID R. VEBLEN

Department of Earth and Planetary Sciences, Johns Hopkins University, Baltimore, Maryland 21218, U.S.A.

### ABSTRACT

High-resolution and analytical transmission electron microscopy have been used to show that “eastonite” from Easton, Pennsylvania, is a submicrometer lamellar mixture of phlogopite and serpentine. Interfaces between the (001) lamellae of the two sheet silicates are generally sharp, with little fine-scale mixed layering. Electron-microscope and electron-microprobe analyses yield compositions that are consistent with a phlogopite-serpentine intergrowth, rather than the hypothetical “eastonite” endmember formula of Winchell (1925). It is shown that this ideal endmember composition was, indeed, synthesized by Hewitt and Wones (1975). However, there are no reported natural occurrences of aluminous micas that correspond to Winchell’s endmember.

The serpentine in “eastonite” is a previously unreported, polysomatic mixture of the lizardite and antigorite structures. Unlike typical antigorite, which has relatively periodic layer offsets, this serpentine can be described as consisting mostly of the lizardite structure, but with occasional paired offsets typical of antigorite. The antigorite offsets occur in three orientations that are related by the symmetry of  $1T$  lizardite.

### INTRODUCTION

The name “eastonite”<sup>1</sup> is generally used to refer to an aluminous trioctahedral mica that is the magnesian counterpart of siderophyllite (Winchell, 1925; Deer et al., 1962; see App. 1 for historical details on the usage of this mineral name). Its endmember formula,  $KMg_{2.5}Al_{0.5}[Si_{2.5}Al_{1.5}O_{10}](OH)_2$ , corresponds to a phlogopite with substantial Tschermaks substitution. Reports of “eastonite” occurrences are rare, with only a few localities having been noted since the turn of the century. Until 1960, micas from Chestnut Hill in Easton, Pennsylvania (Eyerman, 1904), and Dowerin, Western Australia (Simpson, 1932), were believed to approach the “eastonite” endmember composition closely. However, Foster (1960) showed that chemical analyses of these micas do not, in fact, correspond to this composition. In addition, Yoder (unpub., 1957, as noted by Foster, 1960) used powder X-ray diffraction data to show that “eastonite” from the type locality at Easton is a mixture of mica and serpentine. Beatty (1949) also reported a powder X-ray pattern from Easton material in which the strongest peak occurred at 0.730 nm; however, she failed to note that this  $d$  value does not correspond to any interplanar spacing for a mica structure but is consistent with  $d_{001}$  for one-layer serpentine. “Eastonite” occurrences are discussed further in Appendix 1.

In the present study, high-resolution transmission elec-

tron microscopy (HRTEM) and analytical electron microscopy (AEM) have been used to verify that “eastonite” from the type locality is a mixture of phlogopite and serpentine and to clarify the nature of the intergrowth. In the past few years, HRTEM and AEM have been used to investigate intergrowths among a number of different sheet silicates (Page and Wenk, 1979; Veblen and Buseck, 1979, 1980, 1981; Veblen, 1980, 1983a, 1983b; Veblen and Ferry, 1983; Iijima and Zhu, 1982; Lee et al., 1984; Lee and Peacor, 1985; Yau et al., 1984; Ahn and Peacor, 1985, 1986; Ahn et al., 1985; Olives Baños et al., 1983; Olives Baños and Amouric, 1984; Olives Baños, 1985; Spinnler, 1985). Many of these studies report the intercalation of different sheet silicates on the unit-cell scale, commonly referred to as mixed layering. In contrast, in the present case, phlogopite and serpentine are shown to exist as relatively wide, discrete lamellae with only minor mixed-layering disorder at their boundaries.

The serpentine found in “eastonite” is of particular interest in light of recent HRTEM investigations of antigorite (Spinnler et al., 1983; Spinnler, 1985; Mellini, pers. comm.). Unlike the relatively periodic modulations of normal antigorite, much of the serpentine in “eastonite” consists of previously unreported intergrowths of the lizardite and antigorite structures. These intergrowths shed some light on previous structural models for antigorite. In addition, the chrysotile structure occurs in limited amounts in the serpentine lamellae. Thus, all three of the classically recognized serpentine varieties (Whittaker and Zussman, 1956) occur in this specimen.

<sup>1</sup> In this paper, we surround “eastonite” with quotation marks. This usage was suggested by the IMA Commission on New Minerals and Mineral Names (E. H. Nickel, pers. comm., 1985).

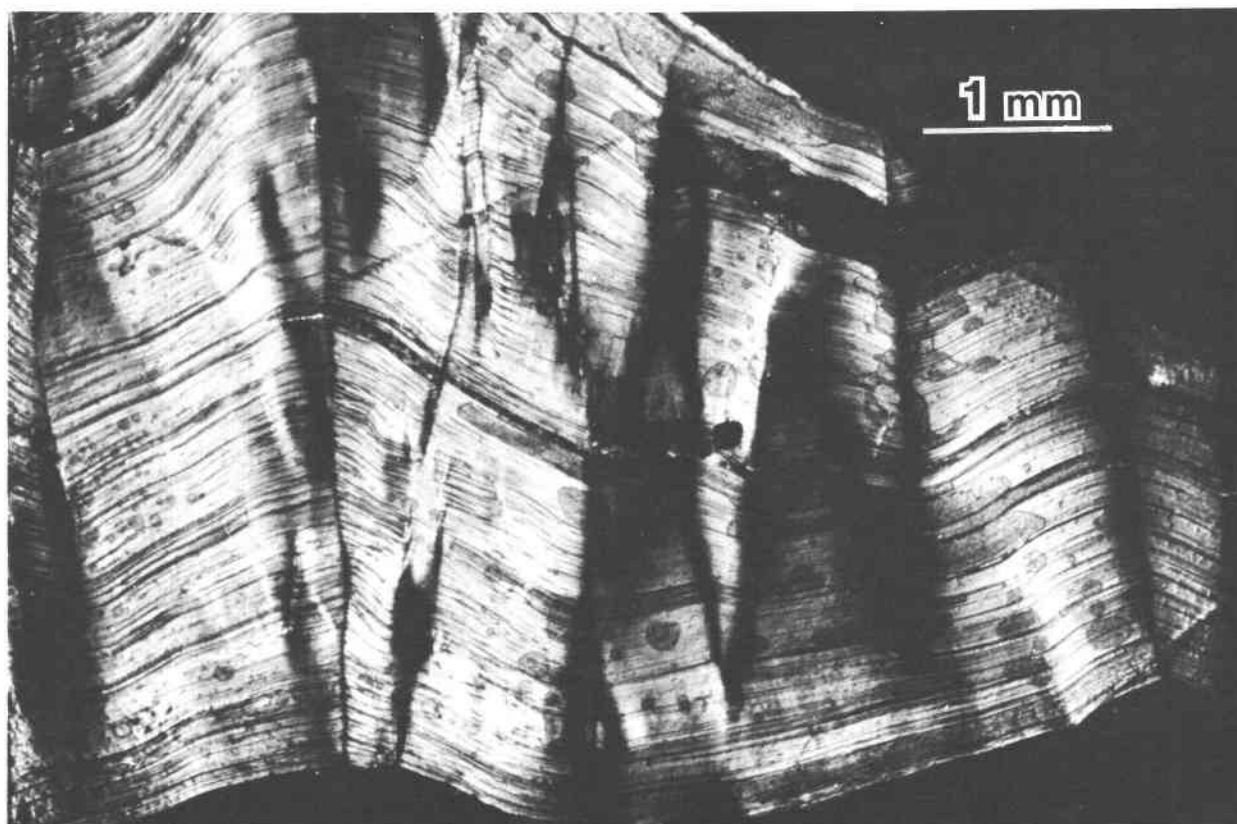


Fig. 1. A light micrograph of "eastonite" from Easton, Pennsylvania, cut normal to the basal planes (crossed polars). Dark areas are at extinction. The sheet silicate is deformed, and light and dark layers in the micrograph are due to variations in interference colors normal to the sheets.

#### SPECIMEN DESCRIPTION, EXPERIMENTAL METHODS, AND IMAGE INTERPRETATION

The specimen employed in this study is number P948 from the mineral collection of Lafayette College, Easton, Pennsylvania, and was kindly supplied by Guy Hovis. In hand specimen, the "eastonite" is white to pale green, and it is colorless in thin section. The basal planes are kinked (Fig. 1), presumably as a result of deformation. In cross-polarized light, the birefringence is observed to vary perpendicular and parallel to the basal planes on a scale from 2 to 25  $\mu\text{m}$ . Backscattered-electron images show that even regions with uniform interference colors are mixtures of at least two minerals.

Electron-transparent foils were prepared by argon ion milling of fragments from petrographic thin sections, followed by coating lightly with carbon. Electron microscopy was performed with a Philips 420ST microscope operated at 120 keV, and a 50- $\mu\text{m}$  objective aperture was used for HRTEM experiments. Unfortunately, the combination of very rapid beam damage and specimen deformation generally precluded precise orientation of specific specimen areas, so that many images are from regions that are slightly out of optimum orientation for HRTEM imaging. Image interpretation follows that used in other HRTEM studies of sheet silicates, as noted in the Introduction, consistent with the image simulations of Amouric et al. (1981) and Spinnler et al. (1984). Interpretation of antigorite images follows that of Spinnler (1985) and Mellini (pers. comm.) and is based on the extensive image simulations of Spinnler.

X-ray analyses in the TEM were obtained with an EDAX energy-dispersive spectrometer (EDS) and a Princeton Gamma-Tech System IV analyzer. AEM was used to obtain analyses from individual phlogopite and serpentine lamellae. A description of the analysis procedures is given in Appendix 2. Electron-microprobe (EMP) analyses and backscattered-electron images were obtained with a Cameca Camebax-microbeam at the State University of New York at Stony Brook. Enstatite, orthoclase, and hornblende were used as standards. AEM and EMP analyses of "eastonite" are reported in Table 1.

Phlogopite lamellae were identified by the presence of high concentrations of Al and K in EDS spectra, by quantitative AEM analyses, and by 1.0-nm (001) periodicities in selected-area electron-diffraction (SAED) patterns and HRTEM images. Serpentine lamellae were identified by low concentrations of Al and K, by quantitative analysis, and by 0.7-nm (001) periodicities in diffraction patterns and images. In a single area, talc was identified by an EDS analysis, but the vast bulk of the specimen consists only of phlogopite and serpentine.

#### COMPOSITION OF "EASTONITE"

The average composition reported in Table 1 was derived from 30 electron-microprobe analyses taken in a traverse of 50- $\mu\text{m}$  steps normal to the basal (001) planes. In order to obtain the best average composition, for each analysis position, the electron beam (approximately 1.5-

Table 1. AEM and EMP analyses of minerals in "eastonite," its bulk composition, and previous analyses

	"Best" phlogopite	"Best" phlogopite	"Best" serpentine	"Best" serpentine	Ideal mixture 70% phlog + 30% serp	Average "eastonite"	"Chloritic vermiculite" Chestnut Hill Clark and Schneider (1891)	"Eastonite" 104 Chestnut Hill Eyerman (1911)
Si	3.1	4.00	3.01	4.00	2.0	2.0	2.03	2.03
Al <sup>IV</sup>	0.9		0.99					3.07
Al <sup>VI</sup>			0.03					0.73
Mg	3.0		2.97		0.02		0.10	3.40
Ti		3.04		3.03	2.9		2.74	3.44
Fe <sup>3+</sup>					2.95		2.85	3.44
Fe <sup>2+</sup>	0.04*		0.03		0.03		0.01	0.04
Mn								0.02(0.01)
Na								0.62
K	0.6	0.6	0.89	0.89	0.06	0.06	0.03	0.65
Ca								0.65
O**	11	11	7	7	11	11	11	11
Method	AEM	EMP	AEM	EMP	AEM/ EMP	EMP	wet chem.	wet chem.
						1σ		
						3.79	2.74	3.01
						0.73(0.11)	0.27	2.69
								0.92
							3.60	2.85
							0.04	3.64
								0.04
								0.03
								0.19
							0.18	0.16
							0.20	0.02
								0.37

\* FeO as total iron.

\*\* Assumed number of oxygens.

μm diameter) was rastered over a 5-μm line normal to (001). In addition to the analyses used to derive this average composition, numerous analyses were collected using a 1–2-μm diameter stationary beam in areas of maximum and minimum K content, as indicated by a ratemeter monitoring the potassium *Kα* X-ray peak.

As shown in Table 1, the average composition is consistent with a mixture of approximately 70% phlogopite and 30% serpentine by volume. To determine these proportions, AEM analyses of the submicrometer serpentine lamellae were used. Although K loss induced by the electron beam caused AEM analyses of phlogopite to be relatively inaccurate, a few of the electron-microprobe spot analyses exhibited good phlogopite stoichiometry; these analyses were averaged and used in the calculation of volume proportion.

Taken together, the electron-microprobe and electron-microscope analyses of the present study show that "eastonite" from the type locality possesses a composition that is consistent with a mixture of serpentine and phlogopite. This composition is very different from that expressed by the hypothetical "eastonite" endmember composition. In fact, the addition of serpentine to phlogopite yields a composition that is even less aluminous than that of a normal trioctahedral mica.

This observed composition is, however, similar to an analysis of a "chloritic vermiculite" from Chestnut Hill in Easton reported by Clarke and Schneider (1891) and an analysis of an altered biotite labeled "eastonite" by Eyerman (1911) (Table 1). These three compositions are plotted on a Si–Al–(Mg + Fe) cation-normalized ternary composition diagram (Fig. 2). Both the observed bulk composition and that of Clarke and Schneider (1891) plot between ideal phlogopite and serpentine, whereas the "eastonite" of Eyerman (1911) does not. It is likely that these three analyses are from similar material; however,

since the specimens analyzed in the earlier studies apparently are not extant, it is not possible to demonstrate rigorously that they are all mixtures of phlogopite and serpentine. It is quite possible that the composition of "eastonite" varies from specimen to specimen, even though the low standard deviations of analyses from sample P948 show that the composition within one sample may be relatively homogeneous at an analytical resolution of 5 μm.

#### TEXTURE AND CRYSTALLOGRAPHY OF "EASTONITE"

"Eastonite" is composed of alternating lamellae of phlogopite and serpentine (Fig. 3). The phlogopite lamellae are generally less than 0.2 μm wide, with some reaching 0.5 μm, and most of the serpentine lamellae are less than 0.15 μm wide, though some are up to 0.3 μm. Based on measurements of lamellar widths in electron micrographs, phlogopite constitutes approximately 70% of the intergrowth by volume, in agreement with the compositional estimate of relative volumes discussed in the last section.

The lamellar interfaces are parallel to the (001) basal planes of both sheet silicates, so that the phlogopite and serpentine share *c\** reciprocal axes (see SAED pattern inset in Fig. 3). Relatively weak, dark contrast at the borders of the lamellae is due to dislocations resulting from minor mismatch between phlogopite and serpentine. The phlogopite is predominantly the 1M polytype, with *a* = 0.53, *c* = 1.02 nm, and β = 100.6°. Most of the serpentine is lizardite, with planar layers, and the corrugated structure of antigorite in places is polysomatically intermixed with the lizardite. Little of the serpentine can be regarded as true antigorite, since the corrugations in antigorite proper are relatively periodic, whereas those in the serpentine of "eastonite" are not. This previously unreported modifi-

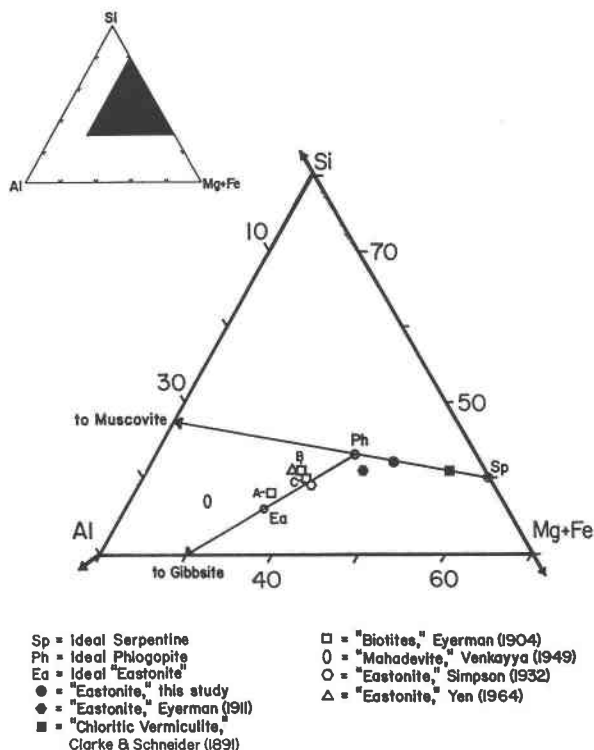


Fig. 2. Compositions of "eastonites," aluminous phlogopites, and altered biotites plotted in a Si-Al-(Mg + Fe) cation-normalized ternary diagram. The large triangle is an expanded view of the shaded portion of the full system. Analyses are given in Table 1 for solid symbols and in Table 3 for open symbols. The letters A, B, and C refer to the labels of Eyerman (1904). The "eastonite" of the present study and the "chloritic vermiculite" of Clarke and Schneider (1891) plot on a line between ideal phlogopite and serpentine. The "eastonite" analysis of Eyerman (1911) is slightly lower in silica than a mixture of phlogopite and serpentine. Analyses of Simpson (1932), Yen (1964), and Eyerman B and C (1904) plot approximately halfway between phlogopite and the "eastonite" endmember composition of Winchell (1925). In this projection, analysis A of Eyerman (1904) plots close to the "eastonite" endmember, but it is not a mica (see App. 1).

cation of the serpentine structure will be discussed in detail in the next section. In addition to the lizardite and lizardite-antigorite, small amounts of chrysotile occur in some of the serpentine lamellae.

SAED patterns obtained parallel to the *b* axis show that the serpentine possesses unit-cell parameters  $a = 0.53$ ,  $c = 0.72$  nm, and  $\beta = 90.5^\circ$  (indexed in terms of a *C*-centered monoclinic unit cell analogous to that used for the phlogopite). In regions where the serpentine appears to be pure lizardite, the measured deviation of  $\beta$  from  $90^\circ$  is generally smaller than the possible error in the electron-diffraction measurements. The observed unit-cell parameters therefore are not inconsistent with a true trigonal symmetry, as observed in lizardite 1*T* by Mellini (1982).

Streaking in the diffraction pattern of Figure 3 is primarily the result of stacking disorder in both the serpentine and the mica. Some of the streaking may also result from minor intercalation of the two structures near their lamellar interfaces.

The mottled or spotty texture of the phlogopite is caused in part by electron-induced damage involving separation of the layers of the structure. The warping of the layers around these separations leads to local differences in diffracting condition and hence contrast of the image (i.e., strain contrast). Similar beam damage is common in other sheet silicates. The lizardite in the present specimen exhibits more rapid damage than the phlogopite; layer separations also occur in lizardite, but commonly the gaps between parted layers close before the serpentine becomes amorphous. Portions of the serpentine that are distorted or curved (chrysotile structure) damage more rapidly than the lizardite and mixed lizardite-antigorite structures.

Light, rectangular features in electron micrographs of the serpentine, arrowed at the left of Figure 3, are of unknown origin. They are not the result of beam damage, being present from the onset of relatively low-dose observation and not changing during observation. Many of these areas have 0.72-nm lattice fringes traversing them that are not offset relative to those of the surrounding serpentine. The lighter contrast of these rectangular features suggests that these areas are thinner than their surroundings; they therefore are most likely voids, perhaps created by very small fluid inclusions. These voids are most abundant in regions with many antigorite offsets.

## SERPENTINE POLYSOMATIC INTERGROWTHS

### Previous work

The serpentine minerals contain layers consisting of a tetrahedral silicate sheet and a Mg-rich trioctahedral sheet. These 1:1 sheet silicates traditionally are divided into three species (Whittaker and Zussman, 1956): lizardite possesses planar layers, the layers of chrysotile are curled, and the corrugated structure of antigorite apparently consists of curved layers with periodic reversals in the sense of curvature (Fig. 4). Although this classification of Whittaker and Zussman is a useful and necessary one, it is now recognized that intimate intermixing of the three different serpentine structures can occur (e.g., Veblen and Buseck, 1979, 1981; Veblen, 1982).

Compared to other common rock-forming silicates, the structure of antigorite is still only poorly known, owing at least in part to a lack of high-quality single crystals for X-ray structure refinement. The best model for the structure is generally considered to be the alternating wave model shown in Figure 4, which in prototype form was initially described by Onsager (see Zussman, 1954, p. 502) and in its details is based primarily on the X-ray work of Kunze (1956, 1958, 1961). As pointed out by Zussman (1954), the silicate sheets of this structure possess six-membered rings at one of the planes where the layer cur-

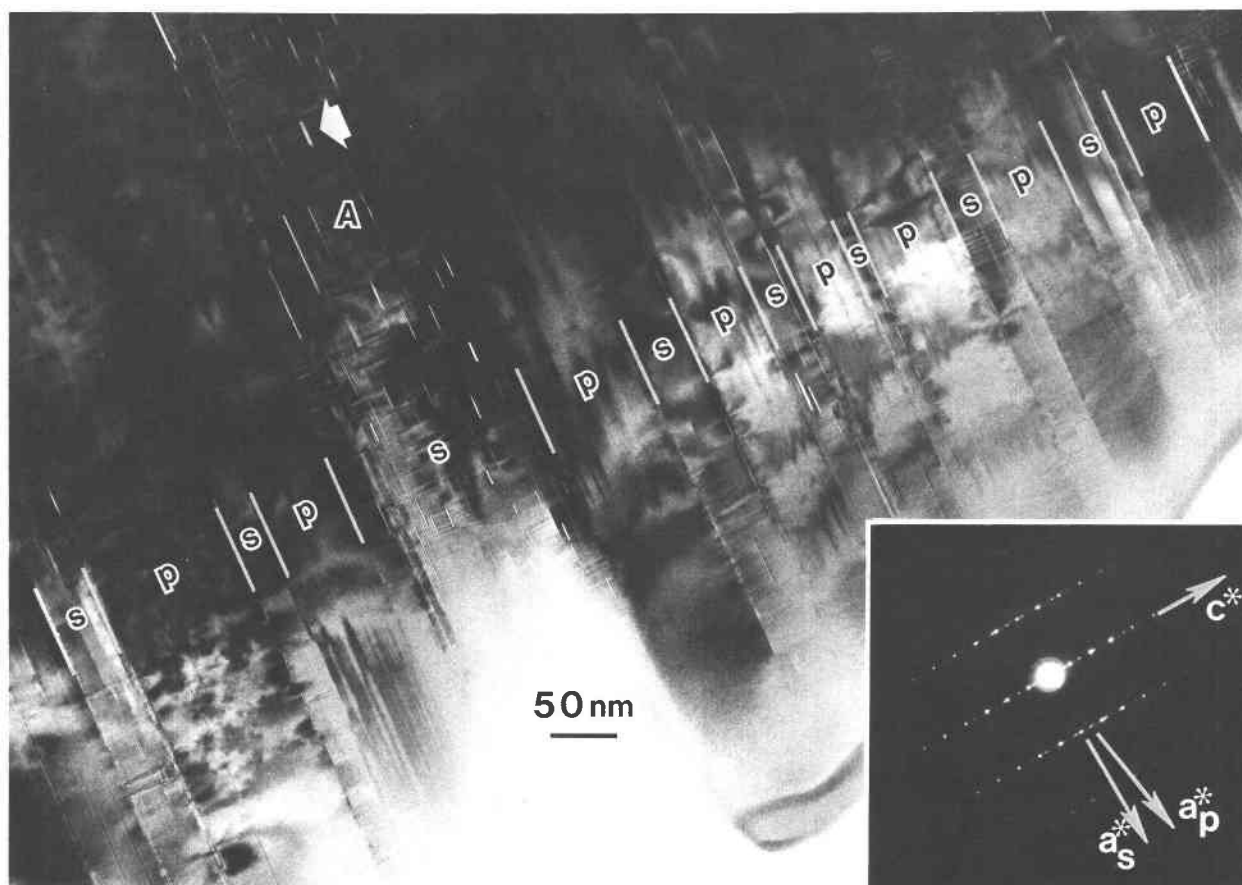


Fig. 3. Overview of an intergrowth of phlogopite (p) and serpentine (s) in "eastonite." The selected-area electron-diffraction (SAED) pattern (inset) shows that phlogopite and serpentine share  $c^*$ ,  $a$ , and  $b$  axes (assuming the  $C$ -centered monoclinic unit-cell setting for the serpentine). See text for discussion of arrowed feature and the lamella labeled A.

vature reverses, but they contain both eight- and four-membered rings at the other reversal (Fig. 5).

As noted by Livi and Veblen (1985) and amplified by Spinnler (1985), the antigorite structure can be thought of as a polysomatic structure (Thompson, 1978) containing three different types of slabs. Two of the slabs lie at the positions of the reversals, and a number of lizardite-like slabs are interleaved between the reversal slabs (Fig. 5). As shown by Spinnler (1985), the two reversal slabs are electrostatically charged, one positively and the other negatively, rather than being neutral. (If the antigorite structure of Kunze is indeed correct, then this represents a highly unusual case in which charge compensation in a silicate occurs over a range of roughly 2.0 to 6.0 nm.) The reversals with six-membered rings possess a different Mg/Si ratio from that of lizardite or chrysotile. Therefore, the antigorite structural formula will vary depending on the number of lizardite-like slabs occurring between reversals.

Investigations of antigorite with HRTEM have yielded images with offsets in the (001) lattice fringes (Yada, 1979; Spinnler, 1985; Mellini, pers. comm.). Using an extensive

set of computer-simulated images, Spinnler (1985) showed that the HRTEM image character for antigorite changes appreciably with small variations in microscope defocus and orientation. However, in spite of this wide variation in image detail, offsets in the (001) fringes occur over a wide range of experimental conditions and correspond to the positions of the slabs of curvature reversal. Furthermore, one of the reversal types undergoes beam damage more rapidly than the other, allowing the two reversal types to be distinguished in experimental images (see Fig. 6). Thus, relatively detailed interpretation of experimental images is commonly possible, in spite of experimental difficulties associated with rapid beam damage and local variations in orientation that are typical of antigorite.

The studies of Spinnler (1985) and Mellini (pers. comm.) have shown that normal antigorites can contain a wealth of defect types. Some variation in the modulation period can occur, owing to different numbers of lizardite-like slabs between reversals. However, previously reported antigorites tend to have rather constant modulation periods, at least locally. As seen below, this is not the case for the serpentine in "eastonite." In addition, the

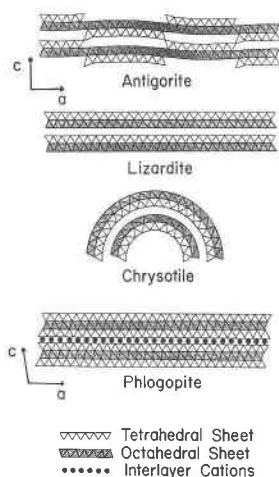


Fig. 4. Simplified diagrams of the structures found in "eastonite" (see Deer et al., 1962, for example). Antigorite is characterized by offsets or reversals in the apical oxygen direction of the tetrahedral sheets, lizardite has planar layers, and chrysotile has curved layers; all of these serpentine minerals have interlayer spacings of approximately 0.72 nm. The mica phlogopite can be distinguished from serpentine in HRTEM micrographs by its interlayer spacing of approximately 1.0 nm and by K in AEM analyses.

reversal slabs in "eastonite" occur in three intersecting orientations, rather than a single orientation parallel to (100) as is typical of normal antigorite.

### Serpentine polysomatism in "eastonite"

Although some of the serpentine in "eastonite" is high-quality lizardite, much of it is a highly disordered intergrowth of the lizardite and antigorite structures. For example, some of the serpentine lamellae in Figure 3 are predominantly lizardite with randomly intergrown, paired antigorite offsets. Although parts of some lamellae possess a density of antigorite offsets that approach that of normal antigorite (see lamella A in Fig. 3), they never exhibit the degree of ordering shown by the antigorites studied by Yada (1979), Spinnler (1985), and Mellini (pers. comm.). In the "eastonite" serpentine, there appears to be no correlation between the lamellar width and the degree of ordering of antigorite offsets.

An important observation made possible by the differential damage rates of the two antigorite offset types is that these offsets invariably occur in pairs (as they do, of course, in the ordered, ideal antigorite structure). In disordered antigorite-lizardite intergrowths, this pairing is not required by the topology of the structure; it is, however, required for charge balance, since the two polysomatic offset slabs are apparently oppositely charged, as noted above. The measured distances between paired offsets range from approximately 1.8 to 6.5 nm. Since the distance between two offsets corresponds to roughly one-half of the antigorite unit cell, these measurements are equivalent to antigorite  $a$  values ranging from approximately 3.2 to 13.0 nm. This spread covers the entire range of unit-cell parameters reported in the literature for nor-

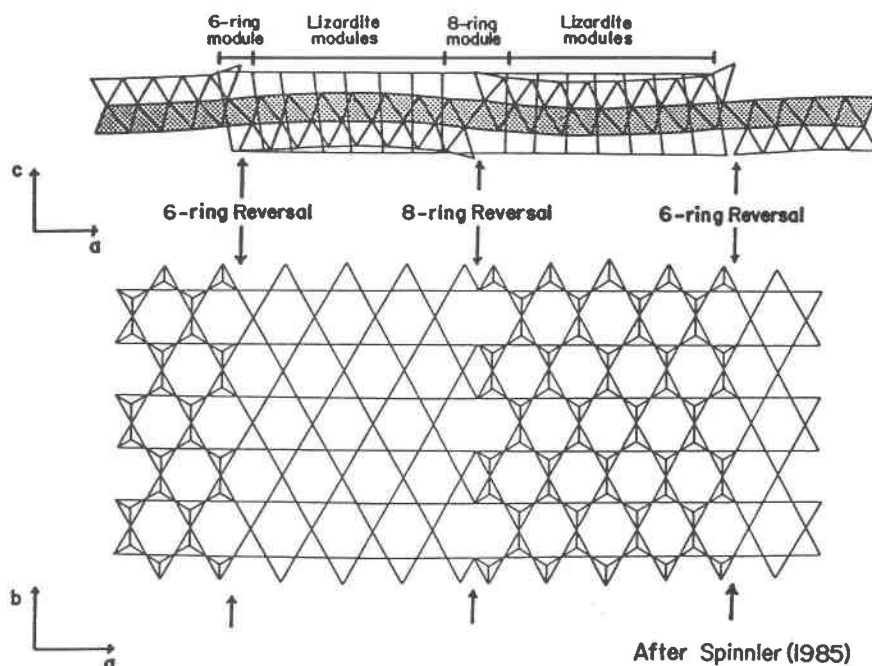


Fig. 5. The polysomatic model of antigorite (Spinnler, 1985), based on the structure of Kunze (1956, 1958). The paired offsets are of two types, one with six-membered rings in the silicate sheets, and the other with eight- and four-membered rings. Between these reversal modules, variable numbers of lizardite-like modules can be placed, resulting in different distances between paired offsets and the reversals of a pair.



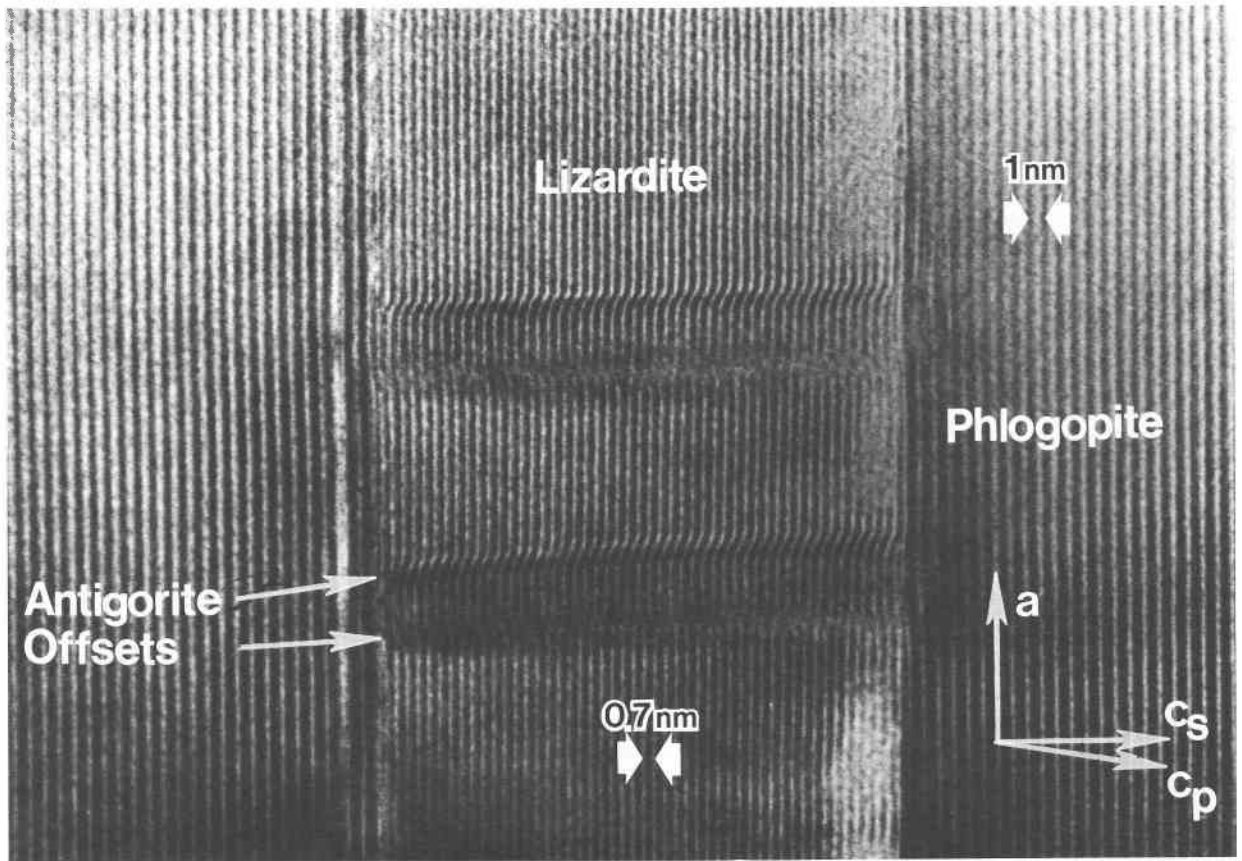


Fig. 6. (above) Experimental HRTEM image of phlogopite, lizardite, and antigorite, which are pervasively intermixed in "eastonite." This region contains two paired offsets, characteristic of the antigorite structure, intergrown in the lizardite. One offset of each pair shows the characteristic beam damage noted by Spinnler (1985).

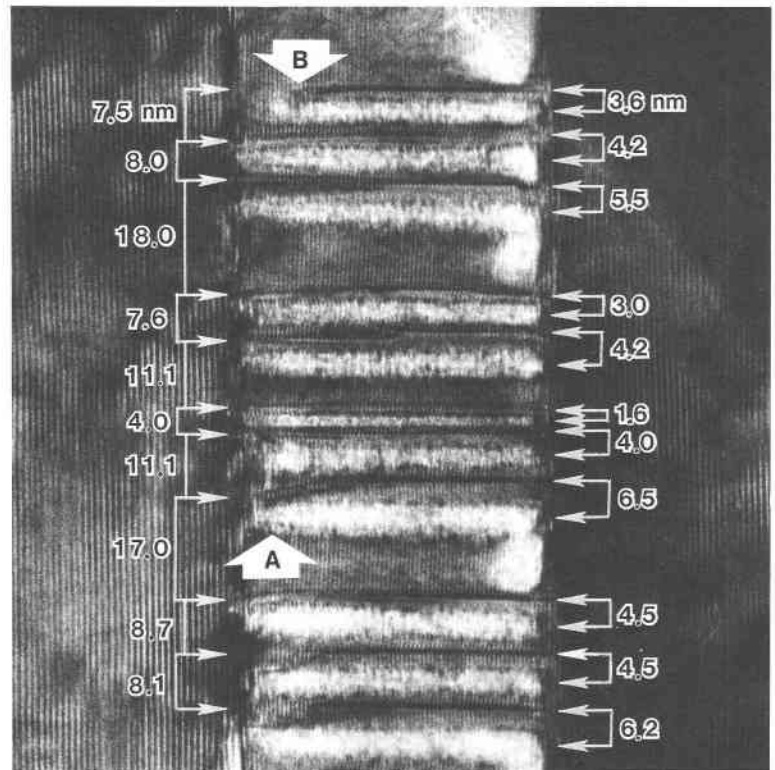


Fig. 7. Experimental image of a polysonic mixture of antigorite and lizardite. Six- and eight-membered-ring offsets always occur in pairs. The distances between paired offsets vary from approximately 1.6 to 6.5 nm, equivalent to antigorite  $a$  axes from 3.2 to 13.0 nm.

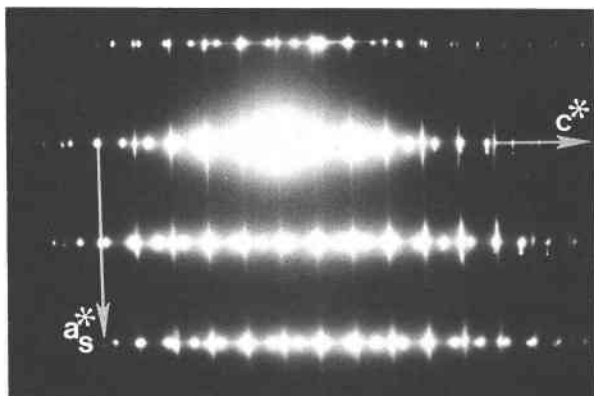


Fig. 8. Electron-diffraction pattern of disordered antigorite-lizardite. The streaking of serpentine diffractions in the  $a^*$  direction is due to disorder in the periodicity of antigorite offsets. The pattern also shows diffractions from adjacent phlogopite.

mal, ordered antigorites. Figure 7 shows a lamella that has both very small and very large spacings between paired offsets in close proximity.

The angle between the (100) planes of offset and the (001) serpentine layers in antigorite is ideally approximately  $91.6^\circ$ . Spinnler (1985) and Mellini (pers. comm.) noted that this angle can be variable, and Spinnler proposed a model for these variations that involves offsets equal to increments of one lizardite module parallel to [100] between adjacent layers. This model accounts both for the angular variation between offset slabs and serpentine layers and for the irrational orientation of satellite spots in diffraction patterns from some antigorites. Offsets in "eastonite" that deviate substantially from the  $91.6^\circ$  angle are shown in area A of Figure 7. A SAED pattern from a serpentine lamellae with a high concentration of

antigorite offsets is shown in Figure 8. The satellite spots are highly streaked, owing to the disorder in the offset spacing. The satellite streaks line up with the substructure diffractions, indicating that the majority of (100) offset planes are near the ideal orientation.

Area B in Figure 7 shows a pair of antigorite offsets that terminate, rather than extending completely across the serpentine lamella. Although most offsets extend across an entire lamella, such terminations are not uncommon in "eastonite." A possible structure for such a termination of offset slabs is shown in Figure 9a. From the diagram, it can be seen that the termination produces a region of talc-like or brucite-like structure, depending on the sense of the termination. Thus, the terminations apparently form structures typical of minerals that commonly are associated with serpentine minerals.

Images taken parallel to the  $c$  axis of the serpentine were obtained from crushed-grain mounts of the Easton material. Previous work on antigorite in this orientation has shown fringes resulting from offsets that are relatively straight and in only one orientation (Hutchison et al., 1977; and unpublished observations by Veblen, 1977). The  $c$ -axis image in Figure 10a shows that the antigorite offsets in the serpentine found in "eastonite" occur in not one but three orientations  $60^\circ$  apart, intersecting to form a pattern of equilateral triangles and other polygons. A SAED pattern from this area (Fig. 10b) shows three sets of diffuse satellites and streaks forming six-pointed stars around each serpentine substructure diffraction; the streaking results from lack of ordering in the spacing between antigorite offsets. This pattern shows that streaks such as those in Figure 8 can occur in three different directions in the  $a^*$ - $b^*$  plane, each direction corresponding to one orientation of disordered antigorite offsets. The occurrence of offsets in three orientations is consistent with true trigonal symmetry for lizardite 1T, as indicated

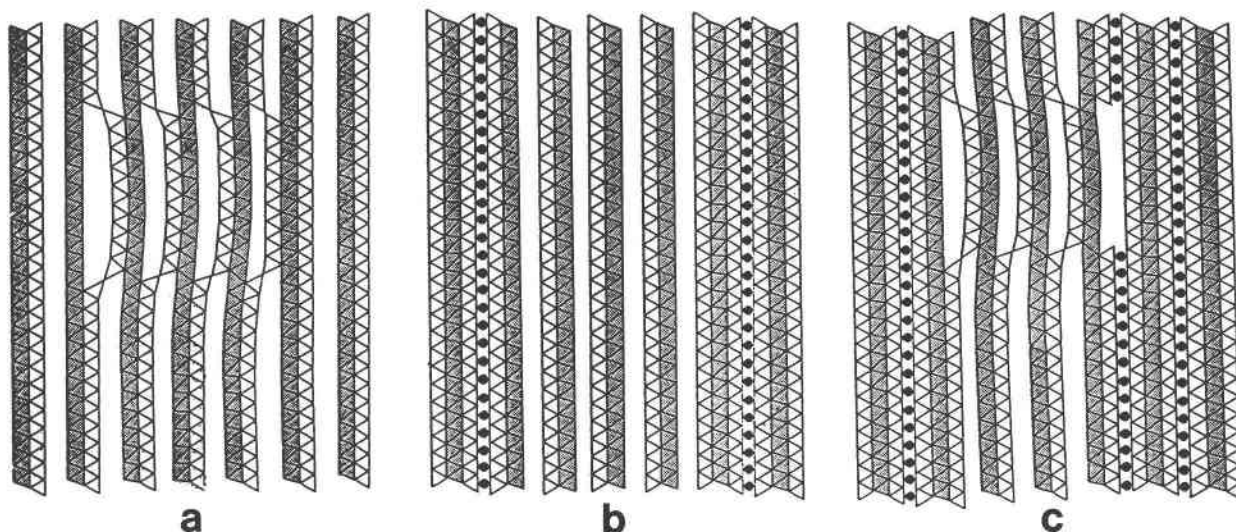


Fig. 9. Schematic diagrams of possible structures of the interfaces in "eastonite." (See Fig. 4 for explanation of symbols.) (a) Termination of paired antigorite offsets in lizardite. (b) Interfaces between phlogopite and lizardite. (c) Interfaces between phlogopite and lizardite containing antigorite offsets.



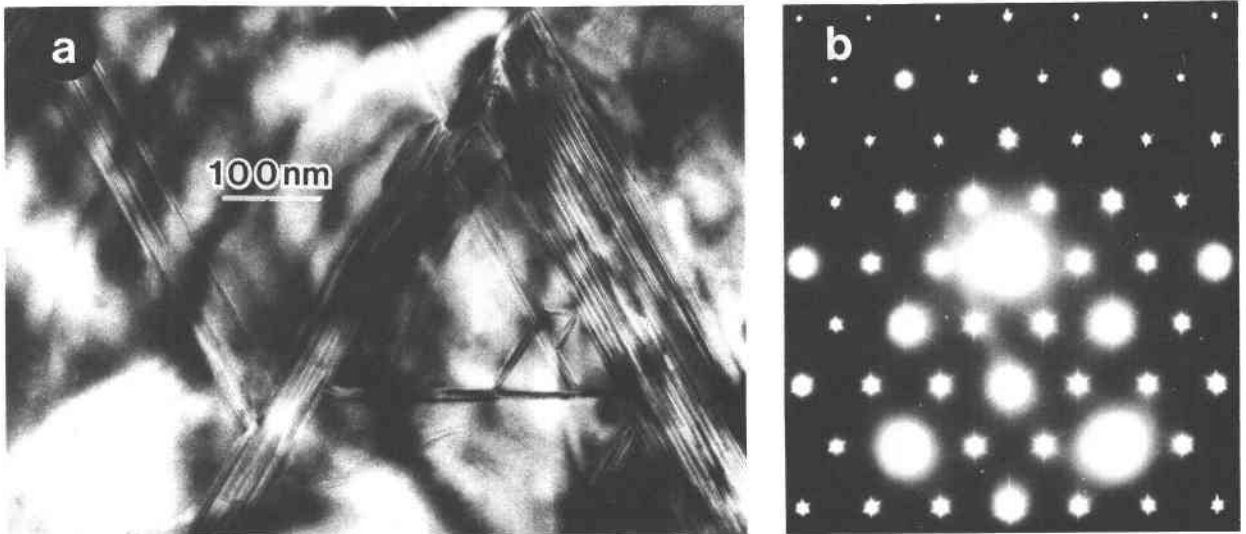


Fig. 10. (a) A c-axis image of antigorite offsets intergrown in lizardite. Unlike the offsets in classical antigorite, which are always parallel, the offsets in the "eastonite" serpentine occur in three orientations 60° apart, resulting from the trigonal or pseudotrigonal character of the lizardite. (b) A c-axis SAED pattern from serpentine in "eastonite." The diffuse satellites and streaks that form six-pointed stars around the lizardite substructure diffractions arise from the occurrence of disordered antigorite offsets in three orientations 60° apart.

by Mellini (1982). The electron-diffraction patterns and the traces of the offsets in images are consistent with offset orientations of (110), (2 $\bar{1}$ 0), and ( $\bar{1}$ 20), indexed in terms of the trigonal lizardite unit cell. In terms of the C-centered monoclinic unit cell used above, the orientations are (100), (310), and ( $\bar{1}$ 30).

#### SERPENTINE-PHLOGOPITE INTERFACES

Because the serpentine in "eastonite" damaged to an amorphous state within a few seconds of exposure to the electron beam and because crystallographic orientation varied slightly on a very fine scale in the TEM specimens, exact adjustment of the orientation of the intergrown phlogopite and serpentine in the electron microscope was generally precluded. Detailed interpretation of the exact interface structures between the two minerals therefore is not possible, because contrast in HRTEM images can be strongly dependent on even minor variations in orientation; the calculations of Spinnler (1985) show that this dependency is especially pronounced for antigorite. However, plausible models for the interface structures can be developed from the structures of the minerals involved.

Figure 9b is a schematic diagram of two lizardite-phlogopite interfaces. Electron-diffraction patterns indicate that there is little mismatch between the two structures, and the sharp lizardite-phlogopite boundaries observed in HRTEM images (Fig. 6) suggest that these minerals fit together with only minor strain. On the other hand, images of antigorite-phlogopite interfaces in places exhibit marked strain contrast (Fig. 7), suggesting that phlogopite is more deformed at these boundaries. A plausible model for antigorite-mica interfaces is presented in Figure 9c. The model requires that some of the apical oxygens of one tetrahedral sheet of a mica layer point

away from the octahedral sheet and instead are bonded to Mg ions of a serpentine layer (left side of diagram). Alternatively, the right side of Figure 9c shows a termination involving a discontinuous silicate sheet in the antigorite layer adjacent to phlogopite, combined with omission of interlayer cations; similar discontinuities in silicate sheets occur in an ordered fashion in the serpentine-related carlosturanite structure (Mellini et al., 1985).

#### SYNTHETIC "EASTONITE"

The substitution of Al in phlogopite has been studied by Crowley and Roy (1964), Hewitt and Wones (1975), and Robert (1976). A review of these studies can be found in Hewitt and Wones (1984). All of these investigations claimed to have synthesized the "eastonite" composition, though no chemical analyses were given (note that the "eastonite" composition as used in the present paper involves only one-half the amount of Tschermak's substitution as that contained in the composition referred to as "Al-eastonite" by Hewitt and Wones, 1975, for example). Synthetic micas typically are sluggish in achieving equilibrium, and runs may not attain 100% yields (Hewitt and Wones, 1984).

Because of this uncertainty in the compositions of synthetic micas and because of the rarity or nonexistence of natural samples having the "eastonite" composition, it is important to establish whether "eastonite" has actually been synthesized. Therefore, the products from two synthesis runs of Hewitt and Wones (1975) were examined using AEM. Results of the energy-dispersive X-ray analyses are presented in Table 2. They show that although each run is somewhat lower in Al content than expected, a mica with a composition close to "eastonite" was, indeed, synthesized. Run 170-70 contains the proper

Table 2. AEM analyses of synthetic "eastonites" of Hewitt and Wones (1975)

	Si	Al <sup>IV</sup>	Al <sup>VI</sup>	Mg	K	Al/Si	
224-69	2.62	1.38	0.39	2.60	1.00	0.68	700°C 1-kbar total pressure
	4.00		2.99				18% difference between Al/Si ratios
Expected composition Hewitt and Wones (1975)	2.50	1.50	0.50	2.50	1.00	0.80	22-d duration 1M polytype
170-70	2.52	1.48	0.53	2.44	1.01	0.80	850°C 1-kbar total pressure
	4.00		2.97				18% difference between Al/Si ratios
Expected composition Hewitt and Wones (1975)	2.38	1.62	0.62	2.38	1.00	0.94	17-d duration 1M polytype

amounts of Al and Si. The Mg content appears to be slightly low, leading to 0.03 vacant octahedral sites. However, taking our analytical accuracy into account, this composition is not distinguishable from the "eastonite" formula.

### DISCUSSION

This study confirms that "eastonite" from the type locality is a mixture of phlogopite and serpentine. The serpentine is a complex, previously unreported polysomatic intergrowth of the lizardite and antigorite structures. Since this peculiar type of serpentine has not been reported before, its occurrence in "eastonite" may be related to the fact that the serpentine is present as narrow lamellae in mica. Although the lizardite-phlogopite interfaces show little evidence of strain, the interfaces between antigorite and the mica give rise to substantial strain contrast in TEM images. Thus, the occurrence as narrow lamellae

constrained by mica may destabilize the antigorite structure relative to the lizardite structure, leading to the observed mixed structure rather than normal antigorite. Alternatively, such intimate mixtures of the antigorite and lizardite structures may eventually prove to be common; to date there have been relatively few studies of the serpentine minerals capable of recognizing such disordered intergrowths.

The microstructures present in "eastonite" do not appear to clarify the origin of the mica-serpentine intergrowth. The serpentine-talc deposits at Easton, from which specimens of "eastonite" have been collected, have experienced a complex history of metamorphism, metasomatism, and deformation (Montgomery, 1955). The material now referred to as "eastonite" has been interpreted as altered biotite or phlogopite (Eyerman, 1911; Gordon, 1922; Montgomery, 1955), and there appears to be no reason to doubt this origin. If "eastonite" did arise by

Table 3. Analyses of selected biotite and "eastonites" from the literature

Eyerman (1904, 1911)						
	Silver-white biotite A(510)	Light-brown biotite B(80)	Dark-brown biotite C(511)	"Eastonite" Simpson (1932)	"Mahadevite" Venkaya (1949)	"Eastonite" Yen (1964)
SiO <sub>2</sub>	41.07	41.12	40.32	35.84	35.42	
Al <sub>2</sub> O <sub>3</sub>	23.34	17.23	18.03	16.68	28.28	
MgO	23.00	24.00	24.79	13.87	16.36	
TiO <sub>2</sub>				0.36		
Fe <sub>2</sub> O <sub>3</sub>	4.35	3.14	5.80	4.14	2.81	
FeO				14.69	1.92	
MnO				0.33		
Na <sub>2</sub> O	1.60	0.42		0.48		
K <sub>2</sub> O	6.30	9.50	10.50	8.48	10.94	
CaO		0.89	0.46		0.74	
H <sub>2</sub> O	0.26	3.56	0.25	4.66	3.72	
Sum	99.92	99.86	100.15	100.49	100.19	
				+F = 0.96		
Cations on the basis of 12 oxygens						
Si	2.92	2.84	2.72	2.71	2.50	2.85
Al <sup>IV</sup>	1.08	1.16	1.28	1.29	1.50	1.15
Al <sup>VI</sup>	0.87	0.24	0.15	0.20	0.85	0.37
Mg	2.43	2.47	2.49	1.56	1.72	1.31
Ti				0.02		
Fe <sup>3+</sup>	0.23	0.16	0.29	0.24	0.15	0.29
Fe <sup>2+</sup>				0.93	0.11	1.03
Mn				0.02		
Na	0.22	0.06		0.07		0.10
K	0.57	0.84	0.90	0.82	0.98	0.81
Ca		0.07	0.03		0.06	
	4.00	4.00	4.00	4.00	4.00	4.00
	3.53	2.87	2.93	2.97	2.83	3.00
	0.79	0.97	0.93	0.89	1.04	0.91

alteration of mica, however, it is of interest that the alteration was pervasive and resulted in a mixture of relatively constant composition in any given specimen, rather than being localized along fractures, as is typically the case for the more brittle chain-silicate members of the biopyribole family. It is also conceivable, though perhaps less likely, that "eastonite" could have formed by primary growth during metamorphism or by the breakdown of another sheet silicate (such as a stoichiometrically equivalent biotite-chlorite mineral as noted by Maresch et al., 1985, and Olives Baños, 1985).

The fact that material from the type locality is a mixture calls into question the use of the name "eastonite." There are no published reports of natural micas having exactly the "eastonite" endmember composition. The closest approach to this composition may be the "mahadevite" of Ramaseshan (1945) and Venkayya (1949), which contains a substantial dioctahedral component (see App. 1). It is clear, however, that "eastonite" can be synthesized and that natural micas can contain appreciable amounts of the "eastonite" component. Following the suggestion of Foster (1960), it seems that "eastonite" should be retained as a useful component for discussions of mica chemistry and petrology, while recognizing that the Easton material from which the name was originally derived is a mixture and does not even possess the "eastonite" composition. It is perhaps unfortunate that the history of this name and its current usage lead to the nonsensical conclusion that "eastonite" is not "eastonite."

#### ACKNOWLEDGMENTS

Guy Hovis kindly supplied specimens of "eastonite" from the mineralogical collection of Lafayette College. We are also indebted to him for useful discussions on the petrology of the Easton area. David Hewitt generously made available synthetic run products from the study of Hewitt and Wones (1975). We thank Gerard Spinnler for discussions on the crystal chemistry of antigorite, and Marcello Mellini kindly provided us with a preliminary manuscript describing his work on antigorite. Paul Bartholomew assisted with electron-microprobe analysis. This research was supported by NSF Grants EAR83-06861 and EAR86-09277 and by a grant from Conoco, Inc. Electron microscopy was performed in the Johns Hopkins HRTEM laboratory, which was established with partial support from NSF Grant EAR83-00365.

#### REFERENCES

- Aden, G.D., and Buseck, P.R. (1979) Rapid quantitative analysis of individual particles by energy dispersive spectrometry. In Dale Newberry, Ed. *Microbeam analysis*, p. 254-258. San Francisco Press, San Francisco.
- Ahn, J.H., and Peacor, D.R. (1985) Transmission electron microscopic study of diagenetic chlorite in Gulf Coast argillaceous sediments. *Clays and Clay Minerals*, 33, 228-236.
- (1986) Transmission and analytical electron microscopy of the smectite-to-illite transition. *Clays and Clay Minerals*, 34, 165-179.
- Ahn, J.H., Peacor, D.R., and Essene, E.J. (1985) Coexisting paragonite-phengite in blueschist eclogite: A TEM study. *American Mineralogist*, 70, 1193-1204.
- Amouric, Marc, Mercuriot, G., and Baronnet, Alain. (1981) On computed and observed HRTEM images of perfect mica polytypes. *Bulletin de Minéralogie*, 104, 298-313.
- Beatty, S. vanD. (1949) X-ray spectrometer study of mica powders. *American Mineralogist*, 34, 74-82.
- Clarke, F.W., and Schneider, E.A. (1891) On the constitution of certain micas, vermiculites and chlorites. *American Journal of Science*, 42, 242-251.
- Cliff, G., and Lorimer, G.W. (1975) The quantitative analysis of thin specimens. *Journal of Microscopy*, 103, 203-207.
- Crowley, M.S., and Roy, Rustum. (1964) Crystalline solubility in the muscovite and phlogopite groups. *American Mineralogist*, 49, 348-362.
- Deer, W.A., Howie, R.A., and Zussman, Jack. (1962) *Rock-forming minerals*, vol. 3. Sheet silicates. Wiley, New York, 270 p.
- Eyerma, John. (1904) Contributions to mineralogy. *American Geologist*, 34, 43-48.
- (1911) *The mineralogy of Pennsylvania*, Part II. Chemical analyses. [Privately published, Easton, Pennsylvania].
- Foster, M.D. (1960) Interpretation of the composition of trioctahedral micas. U.S. Geological Survey Professional Paper 354-B, 11-49.
- Goldstein, J.I. (1979) Principles of thin film X-ray microanalysis. In J.J. Hren, J.I. Goldstein, and D.C. Joy, Eds. *Introduction to analytical electron microscopy*, p. 83-120. Plenum Press, New York.
- Gordon, S.G. (1922) *The mineralogy of Pennsylvania*. Academy Natural Science Philadelphia, Special Publication no. 1, 255 p.
- Guidotti, C.V. (1984) Micas in metamorphic rocks. *Mineralogical Society of America Reviews in Mineralogy*, 13, 357-467.
- Hamilton, S.H. (1899) Exploration of the Delaware Valley. *Mineral Collector*, 6, 117-122.
- Hewitt, D.A., and Wones, D.R. (1975) Physical properties of some synthetic Fe-Mg-Al trioctahedral biotites. *American Mineralogist*, 60, 854-862.
- (1984) Experimental phase relations of the micas. *Mineralogical Society of America Reviews in Mineralogy*, 13, 201-256.
- Hutchison, J.L., Jefferson, D.A., and Thomas, J.M. (1977) The ultrastructure of minerals as revealed by high resolution electron microscopy. *Surface and Defect Properties of Solids*, 6, 320-358.
- Iijima, Sumio, and Zhu, Jing. (1982) Electron microscopy of a muscovite-biotite interface. *American Mineralogist*, 67, 1195-1205.
- Kunze, V.G. (1956) Die Gewellte Struktur des Antigorits, I. *Zeitschrift für Kristallographie*, 108, 82-107.
- (1958) Die Gewellte Struktur des Antigorits, II. *Zeitschrift für Kristallographie*, 110, 282-320.
- (1961) Antigorit. *Fortschritte der Mineralogie*, 39, 206-324.
- Lee, J.H., and Peacor, D.R. (1985) Ordered 1:1 interstratification of illite and chlorite: A transmission and analytical electron microscopic study. *Clays and Clay Minerals*, 33, 463-467.
- Lee, J.H., Peacor, D.R., Lewis, D.D., and Wintsch, R.P. (1984) Chlorite-illite/muscovite interlayered and interstratified crystals: A TEM/STEM study. *Contributions to Mineralogy and Petrology*, 88, 372-385.
- Livi, K.J.T. and Veblen, D.R. (1985) Serpentine and phlogopite intergrowths in "eastonite" from Easton, Pennsylvania. *Geological Society of America Abstracts with Programs*, 17, 645.
- Maresch, W.V., Massonne, H.-J., and Czank, Michael. (1985) Ordered and disordered chlorite/biotite interstratifications as alteration products of chlorite. *Neues Jahrbuch für Mineralogie*, 152, 79-100.
- Mellini, Marcello. (1982) The crystal structure of lizardite 1T: Hydrogen bonds and polytypism. *American Mineralogist*, 67, 587-598.
- Mellini, Marcello, Ferraris, Giovanni, and Campagnone, Roberto. (1985) Carlosturanite: HRTEM evidence of a polysomatic series including serpentine. *American Mineralogist*, 70, 773-781.
- Montgomery, Arthur. (1955) Paragenesis of the serpentine-talc

- deposits near Easton, Pa. Pennsylvania Academy of Science Proceedings, 29, 203–215.
- Myklebust, R.L., Fiori, C.E., and Heinrich, K.F.J. (1978) FRAMEC: A compact procedure for quantitative energy-dispersive electron probe X-ray analysis. National Bureau of Standards Technical Memorandum.
- Olives Baños, Juan. (1985) Biotites and chlorites as interlayered biotite-chlorite crystals. *Bulletin de Minéralogie*, 108, 635–641.
- Olives Baños, Juan, and Amouric, Marc. (1984) Biotite chloritization by interlayer brucitization as seen by HRTEM. *American Mineralogist* 69, 869–871.
- Olives Baños, Juan, Amouric, Marc, De Fouquet, Chantal, and Barronet, Alain. (1983) Interlayering and interlayer slip in biotite as seen by HRTEM. *American Mineralogist*, 68, 754–758.
- Page, R.H., and Wenk, H.-R. (1979) Phyllosilicate alteration of plagioclase studied by transmission electron microscopy. *Geology*, 7, 393–397.
- Ramaseshan, S. (1945) Mahadevite—a new species of mica. *Indian Academy of Science Proceedings A*, 222, 177–181.
- Robert, J.-L. (1976) Phlogopite solid solutions in the system  $K_2O$ -MgO-Al<sub>2</sub>O<sub>3</sub>-SiO<sub>2</sub>-H<sub>2</sub>O. *Chemical Geology*, 17, 195–212.
- Simpson, E.S. (1932) Contributions to the mineralogy of Western Australia—Series VIII. *Royal Society of Western Australia Journal*, 18, 61–74.
- Spinnler, G.E. (1985) HRTEM study of antigorite, pyroxene-serpentine reactions, and chlorite. Ph.D. dissertation, Arizona State University, Tempe, 248 p.
- Spinnler, G.E., Veblen, D.R., and Buseck, P.R. (1983) Microstructure and defects of antigorite. *Electron Microscopy Society of America Proceedings*, 41, 190–191.
- Spinnler, G.E., Self, P.G., Iijima, Sumio, and Buseck, P.R. (1984) Stacking disorder in clinoclinal chlorite. *American Mineralogist*, 69, 252–263.
- Taftø, Johann. (1982) The cation distribution in a (Cr,Fe,Al,Mg)O<sub>3</sub> spinel as revealed from the channelling effect in electron induced X-ray emission. *Journal of Applied Crystallography*, 15, 378–381.
- Thompson, J.B., Jr. (1978) Biopyriboles and polysomatic series. *American Mineralogist*, 63, 239–249.
- Tracy, R.J., and Robinson, Peter. (1987) Origin and metamorphism of sulfidic, graphitic schists. *Wones Volume*, American Journal of Science, in press.
- Veblen, D.R. (1980) Anthophyllite asbestos: Microstructures, intergrown sheet silicates, and mechanisms of fiber formation. *American Mineralogist*, 65, 1075–1086.
- (1982) Intergrowth structures in serpentine minerals. *Australian Conference on Electron Microscopy Proceedings*, 7, 160.
- (1983a) Exsolution and crystal chemistry of the sodium mica wonesite. *American Mineralogist*, 68, 554–565.
- (1983b) Microstructures and mixed layering in intergrown wonesite, chlorite, talc, biotite, and kaolinite. *American Mineralogist*, 68, 566–580.
- Veblen, D.R., and Buseck, P.R. (1979) Serpentine minerals: Intergrowths and new combination structures. *Science*, 206, 1398–1400.
- (1980) Microstructures and reaction mechanisms in biopyriboles. *American Mineralogist*, 65, 599–623.
- (1981) Hydrous pyriboles and sheet silicates in pyroxenes and urallites: Intergrowth microstructures and reaction mechanisms. *American Mineralogist*, 66, 1107–1134.
- Veblen, D.R., and Ferry, J.M. (1983) A TEM study of the biotite-chlorite reaction and comparison with petrologic observations. *American Mineralogist*, 68, 1160–1168.
- Venkayya, E. (1949) A new occurrence of mahadevite. *Indian Academy of Science Proceedings A*, 30, 74–77.
- Whittaker, E.J.W., and Zussman, Jack. (1956) The characterization of serpentine minerals by X-ray diffraction. *Mineralogical Magazine*, 31, 107–126.
- Winchell, A.N. (1925) Studies in the mica group. *American Journal of Science*, 5th ser., 9, 309–327.
- Yada, Keiji. (1979) Microstructures of chrysotile and antigorite by high-resolution electron microscopy. *Canadian Mineralogist*, 17, 679–691.
- Yau, Yu-C., Anovitz, L.M., Essene, E.J., and Peacor, D.R. (1984) Phlogopite-chlorite reaction mechanisms and physical conditions during retrograde reactions in the Marble Formation, Franklin, New Jersey. *Contributions to Mineralogy and Petrology*, 88, 299–306.
- Yen, M.-C. (1964) Hydrothermally altered biotite in molybdenum ores from eastern China. *Acta Geologica Sinica*, 44, 191–212.
- Zaluzec, N.J. (1984) A beginner's guide to x-ray analysis in an analytical electron microscope: Part 1—Quantification K-factor and Si(Li) detector calculations. *Electron Microscopy Society of America Bulletin*, 14, 67–75.
- Zussman, Jack. (1954) Investigation of the crystal structure of antigorite. *Mineralogical Magazine*, 30, 498–512.

MANUSCRIPT RECEIVED MARCH 11, 1986

MANUSCRIPT ACCEPTED SEPTEMBER 2, 1986

#### APPENDIX 1. HISTORICAL USAGE OF THE NAME "EASTONITE"

The usage of the name "eastonite" is not uniform and has changed over the course of this century. Below is a brief summary of the historical details of its usage, which we hope will prevent further confusion. Analyses mentioned here are given in Tables 1 and 3 and are plotted in Figure 2.

The name "eastonite" was first given to what apparently was a vermiculite by Hamilton (1899, as noted in Foster, 1960). Previously, G. P. Merrill of the U.S. National Museum had supplied a "chloritic vermiculite" from a quarry at Chestnut Hill in Easton that was analyzed by Clarke and Schneider (1891). This analysis is similar to the bulk composition of "eastonite" obtained in the present study. In fact, the difference in composition may well be due only to a difference in the proportions of phlogopite and serpentine in the mixture (see Fig. 2).

Eyerma collected and analyzed several sheet-silicate specimens from the Chestnut Hill locality. Among them were three aluminous samples that he called biotites (Table 3, analyses A, B, and C) (Eyerma, 1904). Analysis A, from a silver-white sample, cannot be a mica, since there are more than three octahedral cations in the formula unit, and the interlayer sites are only half filled. The other analyses, B and C, recalculate to be aluminous phlogopites. These three analyses apparently became the subject of confusion in later papers by other workers.

Eyerma (1911) republished analyses A, B, and C with the numbers 510, 80, and 511, and he also included an analysis of an altered biotite from Chestnut Hill that he called "eastonite" (Table 1). The analysis of this "eastonite" is not a perfect mixture of ideal phlogopite and serpentine, but it is sufficiently close to our bulk composition to suggest that it is similar material. At this time, the terms chloritic vermiculite, vermiculite, altered biotite, and "eastonite" were all used by Pennsylvania mineralogists to refer to the same type of material (Gordon, 1922).

Winchell (1925) studied the extent of solid solution in natural biotites. He proposed the name "eastonite" for the Mg analogue of siderophyllite. The name was derived from Easton, Pennsylvania, where Winchell said "Eyerma (1904) found a sample which approaches this composition very closely." Winchell was probably referring to analysis A of Eyerma (1904), which is highly aluminous but clearly is not a biotite. From the time of Winchell's paper to the present, "eastonite" has generally been used to denote the endmember composition given in the Introduction, rather than a term synonymous with altered biotite. (In

some cases, however, petrologists have used the name "eastonite" or "aluminous eastonite" to denote a composition that has twice as much Tschermak substitution as the Winchell end-member—see Hewitt and Wones, 1975, for example.)

There have been few references to occurrences of "eastonite" other than those to material from the Easton area. Yen (1964) reported an "eastonite" formed by alteration of biotite, but his composition is Fe-rich and gives only 1.15 tetrahedral Al cations. Simpson (1932) claimed to have found an Fe-rich "eastonite" in pegmatite veins from Dowerin, Western Australia (Table 3). This analysis and B and C of Eyerman (1904) were reduced to structural formulae by Foster (1960). She showed that these three analyses lack sufficient Al in either the tetrahedral or octahedral sites to even approach the "eastonite" formula. She disregarded Eyerman's analysis A, since it clearly is not that of a mica. (This is rather ironic, given the likelihood that this is the analysis on the basis of which Winchell, 1925, proposed "eastonite" as the name for the mica endmember.) Foster also noted that Yoder (1957, oral comm.) used powder X-ray diffraction to show that "eastonite" from Easton, Pennsylvania, is composed of phlogopite and serpentine. On the basis of an apparent absence of natural examples, Foster (1960) suggested "that the name 'eastonite' be discarded as referring to a natural trioctahedral mica and retained only as a hypothetical end-member."

Foster (1960) apparently was unaware of several aluminous micas found at two localities in India and referred to as "mahadevite" by Ramaseshan (1945) and Venkayya (1949). One of these specimens does possess the degree of Tschermak substitution required by the "eastonite" endmember (Table 3). However, Deer et al. (1962, p. 65) showed that the micas of Ramaseshan and Venkayya also possess substantial substitution of a dioctahedral component. Guidotti (1984) noted that several biotites from sulfide-rich metapelites approach the "eastonite" composition, but reference to the original published analyses shows tetrahedral Al contents substantially below that of the "eastonite" endmember in all cases. Guidotti (1984) also referred to a personal communication from Robinson concerning a similar occurrence of a mica having essentially "eastonite" composition. However, the mica in question recalculates to a tetrahedral Al content of only 1.18, again well below the 1.5 required for "eastonite" (Tracy and Robinson, 1987). It thus appears that although it can be synthesized, a naturally occurring mica with endmember "eastonite" composition has yet to be found.

## APPENDIX 2. AEM PROCEDURES

Analytical electron-microscopy (AEM) analyses were obtained with a Philips 420 transmission-electron microscope fitted with an EDAX lithium-drifted silicon detector inclined 20° to the horizontal. The detector signal was analyzed with a Princeton Gam-

ma-Tech System IV X-ray analyzer. Ion-milled samples were examined in beryllium-cup low-background specimen holders at tilts between 10 and 25°, giving effective take-off angles between 30 and 45°. Analyses were obtained in conventional TEM mode at 120 keV, with spot sizes ranging from approximately 20 to 100 nm in diameter. X-ray background was removed from spectra by scaling and subtracting a floating-reference background spectrum generated from carbon or MnCO<sub>3</sub> (with characteristic Mn peaks removed), using the twist algorithm of Aden and Buseck (1979). Characteristic X-ray peak intensities were obtained by a FRAME-C type Gaussian decomposition (Myklebust et al., 1978). Atomic weight percentages were calculated by the Cliff-Lorimer thin-film ratio method (Cliff and Lorimer, 1975), assuming no absorption or fluorescence effects. The *k* factors with respect to Si for Na, Mg, Al, Ca, Mn, and Fe were empirically derived from ion-milled silicate standards listed by Livi and Reeder (in prep.). The *k* factors for other elements were calculated by the method of Zaluzec (1984).

The errors in AEM analyses are dependent on many factors. Quantitative assessment of some sources of error can be made by observing the variations in intensity ratios for repeated analyses of homogeneous standard samples, by calculating the precisions of empirical *k* factors, and by observing the reproducibility of analyses of standards between different sessions on the electron microscope. Errors that may not be readily assessable can result from factors such as absorption due to anomalous specimen topography; absorption due to analysis of areas too thick to meet the thin-film criterion (e.g., Goldstein, 1979); enhanced X-ray emission due to electron channeling (Taftø, 1982); X-rays entering the detector from areas other than the analysis spot (other parts of the specimen or the specimen holder, for example); and electron-induced loss of certain elements (such as Na and K) from the specimen. These factors largely can be controlled through careful attention to good analytical practices, but they generally account for at least some degradation in analytical precision and accuracy.

Based on repeated analyses of homogeneous standard silicates, the standard deviations of our X-ray intensity ratios are 2% or less for most elements. Likewise, the standard deviations of *k* factors derived from numerous analyses of several standards for each element are 2% or better. Although the precision of analyses obtained under optimum conditions is on the order of 2%, the accuracy of our analyses for most major elements is estimated to be no better than approximately 5% relative to the amount present, owing to the uncertainty in *k* ratios and other factors noted above. For Na and K, the errors may be substantially higher, owing to alkali loss from the specimen during analysis and strong absorption of Na X-rays. Likewise, errors for specimens with high average atomic number in which both light and heavy elements are analyzed can be expected to be worse, owing to differential absorption.